OBLIQUE WAVE SCATTERING BY A RECTANGULAR POROUS FLOATING BREAKWATER WITH SLOTTED SCREENS OVER A SILL-TYPE SEABED

KOTTALA PANDURANGA & SANTANU KOLEY
Department of Mathematics, Birla Institute of Technology and Science-Pilani, Hyderabad Campus, India.

ABSTRACT

In this work, oblique wave scattering by a rectangular porous breakwater with slotted screens floating over a sill-type seabed is examined within the frame of linear wave–structure interaction theory. The Sollitt and Cross model is used to analyze the fluid motion inside the rectangular porous breakwater. In addition, a quadratic pressure jump condition on the slotted screens is adopted to include the effect of wave height on wave attenuation by the slotted screens. The associated physical problem is handled using an iterative boundary element method. Finally, the scattering coefficients such as the reflection, transmission, energy loss coefficients, and wave forces acting on the rectangular porous structure are analyzed for different wave conditions. The time-dependent displacement profiles for the various instants of time are provided. Further, the influence of different geometries of sill-type bottoms on wave scattering is analyzed. The study concludes that the wave forces on the rectangular structure attain their maximum when the distance between the slotted screen and the porous structure is an integral multiple of the wavelength associated with the incident wave for different submergence drafts.

Keywords: energy loss coefficient, iterative BEM, porous breakwater, sill-type seabed, slotted screens.

1 INTRODUCTION

In coastal and harbor engineering, rigid breakwaters are often used to protect shorelines and sea walls from wave attacks. The wave-induced forces on these rigid breakwaters and high wave reflection from the breakwaters significantly affect the durability and stability of the breakwaters. Therefore, for decades, the porous breakwaters have been used to weaken the wave forces and reduce the reflected wave height. Further, these porous breakwaters absorb the incident wave energy and lessen the wave transmission to the lee side of the breakwater to create a tranquility zone (Yu and Chwang [1], Koley *et al*. [2]). In practice, these porous breakwaters are either bottom-mounted or surface-piercing in nature. The bottom-mounted breakwaters require more footprint area and strong bottom foundation and are mostly not suitable for deepwater regions. In contrast, surface-piercing breakwaters occupy a particular area of the total water domain, and they are cost-effective and most suitable for deepwater regions (Tabssum *et al*. [3]).

Several researchers have investigated the problems of water wave interaction with the rigid/porous breakwaters using numerical and analytical approaches based on the linear wave–structure interaction theory (Hu *et al*. [4], Deng *et al*. [5], Koley *et al*. [6], Koley and Panduranga [7]). Mei and Black [8] applied the variational method to study the scattering of gravity waves by rectangular surface-piercing and bottom-founded breakwater under the action of regular normal incident waves. Huang and Chao [9] obtained a regular perturbation solution using a porous Reynolds number for the problem of water wave interaction with a vertical porous breakwater. It was observed from their study that a breakwater with

a larger thickness and smaller Reynolds number transmits less wave energy to the lee side of the breakwater for high-frequency water waves. However, the thickness of the break-water has no significant effect on the reflected wave height. Zhu and Chwang [10] studied the reflection characteristics of a composite porous wave absorber placed over a sloping seaward foundation using the eigenfunction expansion method and the finite difference method. Li *et al*. [11] derived the analytical solutions based on Airy wave theory and exper-imental investigations to analyze the wave reflection from the partially perforated caisson breakwater and wave forces on the vertical porous wall under regular incident wave con-ditions. Tsai *et al*. [12] studied the wave propagation over a submerged porous breakwater placed on a sloping porous seabed. In their study, to handle the associated Boundary Value Problem, a hyperbolic-type time-dependent mild-slope wave equation was derived based on the linearized unsteady flow equation within the porous medium. Wiryanto [13] devel-oped a similar model to Tsai *et al*. [12] to analyze the amplitude reduction phenomena of water waves propagating over a submerged rectangular porous structure using shallow-wa-ter wave equations. Wang and Sun [14] conducted an experimental study to investigate the hydrodynamics of rectangular porous floating breakwater with a mooring system. Most of the analytical solutions require the roots of the dispersion relation in the porous medium. However, the process of finding the complex roots and solving non-self-adjoint eigenvalue problems needs more theoretical efforts. In this regard, Liu and Li [15] presented an analyt-ical solution for obtaining the reflection and transmission coefficients of a surface-piercing porous breakwater without finding the roots of the complex dispersion relation in the porous medium. Koley *et al*. [16] studied the oblique wave trapping by bottom-standing and sur-face-piercing porous structures using the eigenfunction expansion and boundary element method (BEM). In all the aforementioned studies, the bottom seabed was considered uni-form/horizontal in nature. Tabssum *et al*. [3] studied the scattering and trapping of oblique water waves by the bottom-mounted and surface-piercing porous breakwaters having a finite thickness in the seabed undulations. Shen *et al*. [17] and Liu *et al*. [18] analyzed the effect of rectangular sill-type bottom topography on the wave reflection and transmission by an impermeable rectangular floating breakwater. Recently, Panduranga *et al*. [19] analyzed the influence of sill/trench-type seabed in wave interaction with multiple floating vertical slotted screens.

In the present study, an iterative BEM-based numerical solution is presented to study the effect of rectangular, parabolic, and triangular sill-type bottom topography on the scattering coefficients such as the reflection, transmission, and dissipation coefficients and wave loads acting on the floating porous breakwater. Using the Sollitt and Cross model [21], the flow motion inside the porous medium is analyzed. Further, a quadratic pressure jump condition on the slotted screen is adopted to analyze the wave dissipation characteristics by the slotted screens. Finally, using the time series analysis, the free surface displacement profiles due to the presence of rectangular porous breakwater with slotted screens floating over sill-type bottom topography are presented.

2 MATHEMATICAL FORMULATION

The schematic diagram of oblique wave scattering by the rectangular porous breakwater with slotted screens (breakwater system) floating over a sill-type seabed is shown in Fig. 1. A 3D Cartesian coordinate system is considered with the -plane being taken as a horizontal plane and the z-axis being taken vertically upward to analyze the performance of the break-water system under the assumption of the linear wave–structure interaction theory. A porous

Figure 1: Sketch of a floating breakwater system over a sill-type seabed.

breakwater of width B floating at the mean water surface $z = 0$ with the submergence draft d from $z = 0$ and two slotted screens of negligible thickness with submergence depth d are placed as shown in Fig. 1. Let w_1 be the gap length between the slotted screen and porous breakwater, as shown in Fig. 1. The flow regions of the present problem are represented by 1, 2, 3, and 4, as seen in Fig. 1. Further, the fluid is assumed to be incompressible, inviscid, and its motion is irrotational.

Then, the velocity potential Φ_j (x,y,z,t) in every region is expressed as $\Phi_j(x,y,z,t) = \mathrm{Re}\left\{\phi_j(x,z)e^{-\mathrm{i}(vy-\sigma t)}\right\}$, where $\phi_j(x,z)$ satisfies the reduced wave equation ([3]).

$$\left(\frac{\partial^2}{\partial x^2} + \frac{\partial^2}{\partial z^2} - v^2\right)\phi_j = 0, \quad j = 1, 2, 3, 4. \tag{1}$$

Here, the subscript j denotes j^{th} region and $v = k_0 \sin\theta$. k_0 is the wavenumber associated with plane gravity wave, and θ is the angle of incidence. Further, the free-surface BC (boundary condition) at $z = 0$ is given by the equation ([6], [7]):

$$\frac{\partial\phi^{(j)}}{\partial z} = \begin{cases} K\phi^{(j)}, & \text{on } S_{Fj} \text{ for } j = 1, 2, 4, \\ K(m+\mathrm{i}f)\phi^{(j)}, & \text{on } S_{Fj} \text{ for } j = 3, \end{cases} \tag{2}$$

with $K = \sigma^2/g$, g is the acceleration constant. The interface BCs between regions 1, 2, 3, and 4 are expressed as in the equation ([26]):

$$\phi_1 = \phi_j, \quad \frac{\partial\phi_1}{\partial z} = \frac{\partial\phi_j}{\partial z}, \quad \text{on } S_I, \text{ for } j = 2, 4, \tag{3}$$

$$\phi_j = (m+\mathrm{i}f)\phi_3, \quad \frac{\partial\phi_j}{\partial n} = -\epsilon\frac{\partial\phi_3}{\partial n}, \quad \text{on } S_p, \text{ for } j = 1, 2, 4, \tag{4}$$

where $S_p = S_{p1} \cup S_{p2} \cup S_{p3}$ (as shown in Fig. 1). Here, m and f are the inertial and friction coefficients, respectively, and $\in$ is the porosity of the rectangular block. Here, n is the outward normal to the corresponding boundary. The no-flow condition on the seabed is given by the equation ([16]):

$$\frac{\partial \phi_1}{\partial n} = 0, \quad \text{on } S_B. \tag{5}$$

In the past, the linear Darcy model was widely used to model the wave past perforated/slotted barriers. However, this model is not suitable for the fluid flow with a high Reynolds number and KC number where the turbulence-induced energy loss is not considered (Chwang and Chan [25]). To address the turbulence-induced energy loss, many studies have proposed a quadratic porosity model instead of a linear Darcy model ([20]). The quadratic pressure loss condition and the continuity of horizontal velocity normal to the slotted screen are given by the equation ([20]):

$$\begin{cases} \phi_1 - \phi_2 = \alpha_1 \left| \dfrac{\partial \phi_1}{\partial x} \right| \dfrac{\partial \phi_1}{\partial x} + \beta_1 \dfrac{\partial \phi_1}{\partial x}, \\ \qquad\qquad \dfrac{\partial \phi_1}{\partial x} = \dfrac{\partial \phi_2}{\partial x}, \end{cases} \quad \text{on } S_1, \tag{7}$$

$$\begin{cases} \phi_4 - \phi_1 = \alpha_2 \left| \dfrac{\partial \phi_4}{\partial x} \right| \dfrac{\partial \phi_4}{\partial x} + \beta_2 \dfrac{\partial \phi_4}{\partial x}, \\ \qquad\qquad \dfrac{\partial \phi_4}{\partial x} = \dfrac{\partial \phi_1}{\partial x}, \end{cases} \quad \text{on } S_2, \tag{8}$$

with $\alpha_1 = -\dfrac{8i}{3\pi\omega} \dfrac{1-\epsilon_1}{2\mu\epsilon_1^2}$, $\beta_1 = -2C_1$, $\alpha_2 = -\dfrac{8i}{3\pi\omega} \dfrac{1-\epsilon_2}{2\mu\epsilon_2^2}$, and $\beta_2 = -2C_2$. Here, $\in_1$ and $\in_2$ are the porosities of the first (S_1) and second (S_1) slotted screens, respectively, μ is the discharge coefficient, and C_j ($j = 1, 2$) are the blockage coefficients. The expression for C_j ($j = 1, 2$) is as in the following equation ([20], [22]):

$$C_j = 0.5\delta\left(\frac{1}{\epsilon_j} - 1\right) + \frac{s}{\pi}\left\{1 - \ln \epsilon_j + \frac{1}{3}\epsilon_j^2 + \frac{281}{180}\epsilon_j^4\right\}, \tag{9}$$

In which δ and s are the thickness of the screen and the gap between the centers of two neighboring slots ([17]), respectively. Finally, the far-field BCs on $S_{-\infty}$ and S_{∞} are given by the equations ([26]):

$$\lim_{x \to -\infty}\left(\frac{\partial\left(\phi_1 - \phi_0\right)}{\partial x} + ik_0 \cos\theta\left(\phi_1 - \phi_0\right)\right) = 0, \tag{10a}$$

$$\lim_{x \to \infty}\left(\frac{\partial\phi_1}{\partial x} - ik_0 \cos\theta\, \phi_1\right) = 0, \tag{10b}$$

where $\phi_0 = -\dfrac{igA}{\omega} e^{ik_0 \cos\theta x} \psi_0(z)$, $\psi_0(z) = \dfrac{\cosh k_0(z+h)}{\cosh k_0 h}$, and k_0 is the real positive root of

$K = k \tanh kh$.

3 SOLUTION METHOD

3.1 Formulation of integral equations

Applying Green's second identity to the velocity potential ϕ_j and the fundamental solution G, we get ([24])

$$\frac{1}{2}\phi_j(x_0, z_0) = \int_\Gamma \left(\phi_j(x, z) \frac{\partial G}{\partial n} - G \frac{\partial \phi_j(x, z)}{\partial n} \right) dS(x, z), \tag{11}$$

where Γ is the associated boundary of the computational domain. The fundamental solution satisfies the equation:

$$\left(\frac{\partial^2}{\partial x^2} + \frac{\partial^2}{\partial z^2} - v^2 \right) G = \hat{\delta}(P' - Q'),$$

where $\hat{\delta}$ is the Dirac delta function. The fundamental solution G is given by the equation:

$$G = -\frac{1}{2\pi} K_0(k_0 \sin\theta\, r), \quad r = dist(P', Q').$$

Here, r is the distance between the source point $P'(x_0, z_0)$ and field point $Q'(x, z)$. K_0 is the zeroth-order modified Bessel function of the second kind. The normal derivative of the fundamental solution G can be derived analytically in terms of the first-order modified Bessel function of the second kind K_1 ([16]). Substituting eqns (2)–(10) into eqn (11), we get the following integral equations ([19]):

$$-\frac{1}{2}\phi_1 + \int_{S_{-\infty}} \left(\frac{\partial G}{\partial n} - ik_0 \cos\theta\, G \right)\phi_1\, ds + \int_{S_B} \frac{\partial G}{\partial n}\phi_1\, ds + \int_{S_\infty} \left(\frac{\partial G}{\partial n} - ik_0 \cos\theta G \right)\phi_1 ds$$

$$+ \int_{S_{F1}} \left(\frac{\partial G}{\partial n} - KG \right)\phi_1 ds + \int_{S_I US_{P2} US_1} \left(\phi_1 \frac{\partial G}{\partial n} - G \frac{\partial \phi_1}{\partial n} \right) ds \tag{12}$$

$$+ \int_{S_2} \left(\phi_4 \frac{\partial G}{\partial n} + \left(Y_2 \frac{\partial G}{\partial n} + G \right)\frac{\partial \phi_4}{\partial n} \right) ds = \int_{S_\infty} \left(\frac{\partial \phi_0}{\partial n} - ik_0 \cos\theta\, \phi_0 \right) G ds,$$

$$-\frac{1}{2}\phi_2 + \int_{S_1} \left(\phi_1 \frac{\partial G}{\partial n} + \left(Y_1 \frac{\partial G}{\partial n} + G \right)\frac{\partial \phi_1}{\partial n} \right) ds + \int_{S_I} \left(\phi_1 \frac{\partial G}{\partial n} + G \frac{\partial \phi_1}{\partial n} \right) ds$$

$$+ \int_{S_{P1}} \left(\phi_2 \frac{\partial G}{\partial n} - G \frac{\partial \phi_2}{\partial n} \right) ds + \int_{S_{F2}} \left(\frac{\partial G}{\partial n} - KG \right)\phi_2\, ds = 0, \tag{13}$$

$$-\frac{1}{2}\phi_3 + \int_{S_{P1}} \left(\frac{1}{(m+\mathrm{i}f)}\phi_2\frac{\partial G}{\partial n} + \frac{G}{\epsilon}\frac{\partial \phi_2}{\partial n} \right)ds + \int_{S_{P2}} \left(\frac{1}{(m+\mathrm{i}f)}\phi_1\frac{\partial G}{\partial n} + \frac{G}{\epsilon}\frac{\partial \phi_1}{\partial n} \right)ds$$

$$+ \int_{S_{P3}} \left(\phi_3\frac{\partial G}{\partial n} - G\frac{\partial \phi_3}{\partial n} \right)ds + \int_{S_{F3}} \left(\frac{\partial G}{\partial n} - K(m+\mathrm{i}f)G \right)\phi_3 ds = 0, \tag{14}$$

$$-\frac{1}{2}\phi_4 + \int_{S_{P3}} \left((m+\mathrm{i}f)\phi_3\frac{\partial G}{\partial n} + \epsilon G\frac{\partial \phi_3}{\partial n} \right)ds + \int_{S_I} \left(\phi_1\frac{\partial G}{\partial n} + G\frac{\partial \phi_1}{\partial n} \right)ds$$

$$+ \int_{S_2} \left(\phi_4\frac{\partial G}{\partial n} - G\frac{\partial \phi_4}{\partial n} \right)ds + \int_{S_{F4}} \left(\frac{\partial G}{\partial n} - KG \right)\phi_4 \, ds = 0. \tag{15}$$

The expressions for Y_1 and Y_2 are given by the equation:

$$Y_1 = -\left(\alpha_1 \left|\frac{\partial \phi_1}{\partial n}\right| + \beta_1 \right) \text{ and } Y_2 = -\left(\alpha_2 \left|\frac{\partial \phi_4}{\partial n}\right| + \beta_2 \right).$$

Now, we apply the BEM to discretize the aforementioned boundary integral eqns (12)–(15) to solve them numerically for obtaining the unknown velocity potentials and their normal derivatives. In the BEM technique, first, each boundary S_j is divided into N segments that are often termed as the boundary elements. In the present study, for discretizing the boundary integral eqns (12)–(15), the constant BEM approach is adopted in which the values of ø and ϕ and $\partial \phi / \partial n$ are assumed to be constants over each boundary element and equal to the value at the midpoint of each element. On the contrary, the remaining terms that need to be integrated are $\int G\,dx$ and $\int \partial G / \partial n\,dx$. These terms are called influence coefficients, which are calculated analytically ([24]). Now, to generate an equal number of equations as the number of unknowns, the method of point collocation is used with the source point P' (x_0, z_0) running over the midpoints of each boundary element. This yields a system of linear algebraic equations that can be solved by Gauss elimination. It is to be noted that for constant BEM, the boundary is always 'smooth' at the nodal points, and hence the multiplier of ø$_j$ is taken ½ in equation (11). Due to the presence of nonlinearity in the BCs (eqns (7) and (8)), the direct BEM approach cannot be applied. Therefore, an iterative procedure is chosen, as mentioned in refs. [20] and [22]. To obtain the desired convergence, the error limit is taken as $\leq 10^{-4}$, and the required number of iterations is about 10–20. After obtaining the velocity potentials and their normal derivatives, we can obtain the reflection coefficient K_R and transmission coefficient K_T as expressed in the following equations:

$$K_R = \left| -1 + \frac{1}{\Delta^2}\frac{\mathrm{i}\sigma}{gA}e^{\mathrm{i}k_0 \cos\theta l}\int_{-h}^{0}\phi_1(-l,z)\psi_0(z)dz \right|, \tag{16}$$

$$K_T = \left| \frac{1}{\Delta^2}\frac{\mathrm{i}\sigma}{gA}\int_{-h}^{0}\phi_1(r,z)\psi_0(z)dz \right|, \tag{17}$$

where $\Delta^2 = \int_{-h}^{0}\psi_0^2(z)dz$. Further, A is the amplitude associated with an incoming wave. The energy loss coefficient E_{loss} is given by the equation (see ref. [7] for derivations):

$$E_{loss} = \left(1 - K_R^2 - K_T^2\right).$$

(18)

The nondimensional wave loads acting on the porous rectangular structure are given by the equation:

$$F_x = \left| \frac{\omega}{gh^2}(m + \mathrm{i}f) \int_{S_{p1}} \phi_3\, n_x\, d\Gamma \right|, \quad F_z = \left| \frac{\omega}{gh^2}(m + \mathrm{i}f) \int_{S_{p2}} \phi_3 n_z\, d\Gamma \right|.$$

(19)

Here, F_x and F_z are the horizontal and vertical wave forces.

The free surface elevation $\eta(x)$ at $z = 0$ is evaluated using the following equation:

$$\eta(x) = \frac{i\omega}{g}\phi_j, j = 1, 2, 3, 4.$$

(20)

4 VALIDATIONS

In this section, as a limiting case of the present model, the theoretical results of Abul-Azm and Gesraha [23] are compared with the present iterative BEM-based numerical results. Abul-Azm and Gesraha [23] examined oblique wave scattering by a rigid rectangular floating breakwater over a horizontal seabed. It is to be noted that when $m = 1.0, f = 0.0$, and $\in$ = 0.0, the porous floating breakwater behaves like rigid and slotted screens that will disappear when $\alpha_j = \beta_j = 0$ (*j = 1, 2*). For validating the present numerical results with Abul-Azm and Gesraha [23], the variation of the reflection coefficient K_r and transmission coefficient K_t as a function of nondimensional wave number K_0h is plotted in Fig. 2 for two different values of angle of incidence, i.e. $\theta = 0°, 60°$. It is observed that the present iterative BEM-based numerical results are in good agreement with the theoretical results of Abul-Azm and Gesraha [23].

5 RESULTS AND DISCUSSIONS

Here, various results associated with the oblique wave scattering by the rectangular porous breakwater with slotted screens floating over a sill-type seabed are presented. The physical parameters that are considered as $h = 10$ *m* (water depth), $k_0h = 1.0, 2.0, B = 2.0\ h, w_1 = 0.25$ $h, w_r = 1.0\ h, h_1 = 0.75\ h, \theta = 30°$, and $\in_1 = \in_2 = 20\%, m = f = 1.0, \in = 15\%, \mu = 0.5$ are kept constants. Further, the bottom bed profile is taken as expressed in the following equation (see ref. [19]):

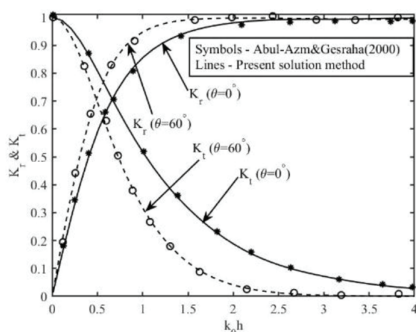Figure 2: Validation of current BEM solution with theoretical results of Abul-Azm and Gesraha [23] with *B/h* = 2.0, *d/h* = 0.25, $\theta = 0°, 60°$.

$$h(x) = \begin{cases} -h, & \left(-l < x < -w_r\right) \cup \left(w_r < x < r\right), \\ -h_1 - \left(h - h_1\right)\left(\dfrac{-x}{w_r}\right)^{\alpha}, & -w_r < x < 0, \\ -h_1 - \left(h - h_1\right)\left(\dfrac{x}{w_r}\right)^{\alpha}, & 0 < x < w_r. \end{cases}$$

Here, h_1 is the gap between the center of the sill and mean free surface ($z = 0$), and l and r are the left and right far-field boundaries, respectively. In general, these far-field boundaries are located two to three times far away from the breakwater system. Depending on the parameter α, the shape of the sill profile will change, i.e. $\alpha = 1.0$ corresponds to the triangular sill, $\alpha = 2.0$ corresponds to the parabolic sill, and $\alpha = \infty$ corresponds to the rectangular sill [19].

5.1 Convergence study

The convergence of the numerical solutions based on the BEM depends on the panel size, which is used to discretize the boundaries of the domain. The panel size is expressed as ([26, 27])

$$p_s = \frac{1}{\kappa k_0},$$

where κ is a proportionality constant that can be obtained from the convergence analysis. Table 1 shows the convergence of the numerical solutions based on BEM for the present problem for various porosities of the floating breakwater. It is seen that for $\kappa \geq 20$, the values of the reflection coefficient K_R and transmission coefficient K_T converge up to four decimal places. Therefore, for the sake of convergence of the present numerical results, the panel size P_s is taken with $\kappa = 20$ for the computational purpose.

5.2 Effect of angle of incidence

In Figs. 3(a)–(d), K_r, E_{loss}, F_x, and F_z versus k_0h (the nondimensional wavenumber) are plotted for the various angle of incidence. Figure 3(a) depicts that the reflection coefficient K_r increases with an increase in θ. Further, with an increase in k_0h, K_r reaches the global maximum and then starts to decrease and reaches the global minima. The global minima shift toward the right

Table 1: Convergence of numerical solution for various porosity porous floating breakwater (ϵ) with $k_0h = 1.0$ and $\alpha = 2.0$ (parabolic sill).

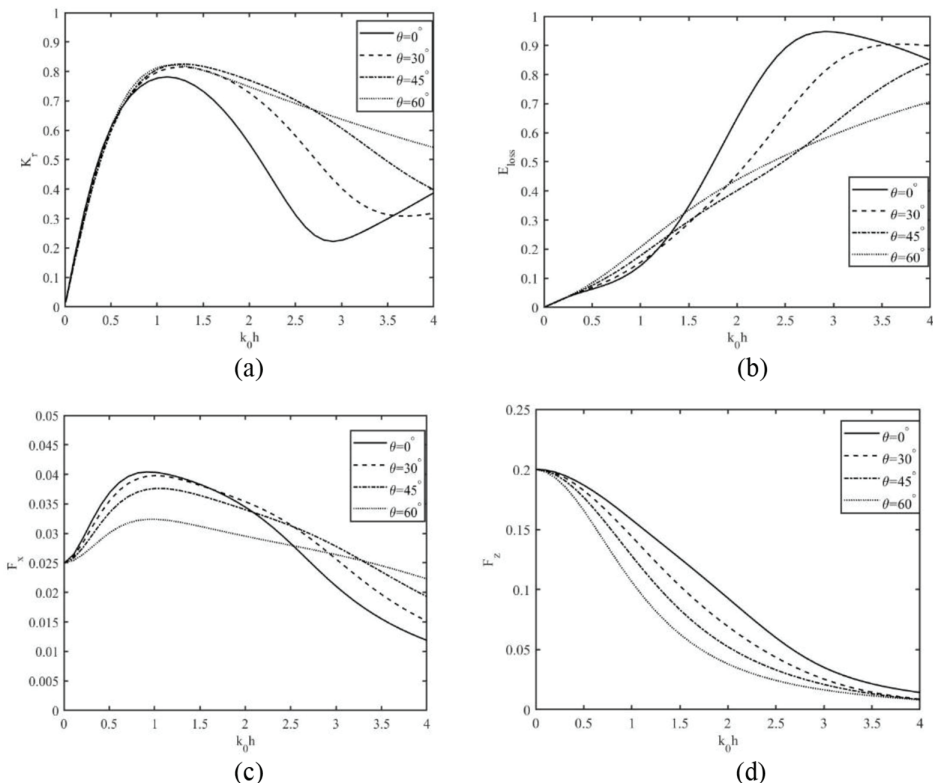| κ	$\epsilon = 0.05$		$\epsilon = 0.15$		$\epsilon = 0.25$		$\epsilon = 0.35$	
	K_R	K_T	K_R	K_T	K_R	K_T	K_R	K_T
5	0.80187	0.50989	0.70546	0.53701	0.62195	0.55881	0.54669	0.57479
10	0.79957	0.52031	0.70418	0.54719	0.62045	0.56913	0.54437	0.58551
20	0.79854	0.52349	0.70320	0.55362	0.61866	0.57277	0.54259	0.59246
30	0.79856	0.52347	0.70320	0.55364	0.61864	0.57276	0.54250	0.59249

Figure 3: Variations of (a) K_r, (b) E_{loss}, (c) F_x, and (d) F_z versus $k_0 h$ for different angles of incidence over a parabolic sill.

for larger values of the angle of incidence θ. Figure 3(b) shows that the energy loss coefficient E_{loss} increases with an increase in the angle of incidence θ for $0.5 < k_0 h < 1.5$. Further, in the intermediate wave regime, E_{loss} decreases for larger values of θ. In Fig. 3(c), the nondimensional horizontal force acting on the porous breakwater F_x decreases with an increase in θ for $0.0 < k_0 h < 2.0$. This happens like a major amount of incoming wave energy is attenuated by the slotted screens. On the contrary, contradictory behavior is noticed in the shortwave regime. Further, the vertical wave forces on the porous structure decrease with an increase in θ.

5.3 Effect of bottom topography

In Figs. 4(a)–(d), K_r, K_t, E_{loss}, and F_x are plotted as a function of the nondimensional wavenumber $k_0 h$ for various seabed profiles. It is observed that the effects of bottom topography on K_r, K_t, E_{Loss}, and F_x are insignificant in the shortwave regime. However, in the longwave regime, the reflection coefficient K_r takes the higher values as $\alpha \rightarrow \infty$, i.e. for rectangular sill. Figure 4(b) shows that K_t decreases as $\alpha \rightarrow \infty$ for $0 < k_0 h < 2.0$. Thus, the proposed breakwater system is effective in the creation of a tranquility zone on the lee side of the breakwater system when it is floating over the rectangular sill, especially in the longwave regime. More than 85% of the incident wave energy is dissipated irrespective of the shapes of the bottom topographies in the shortwave regime.
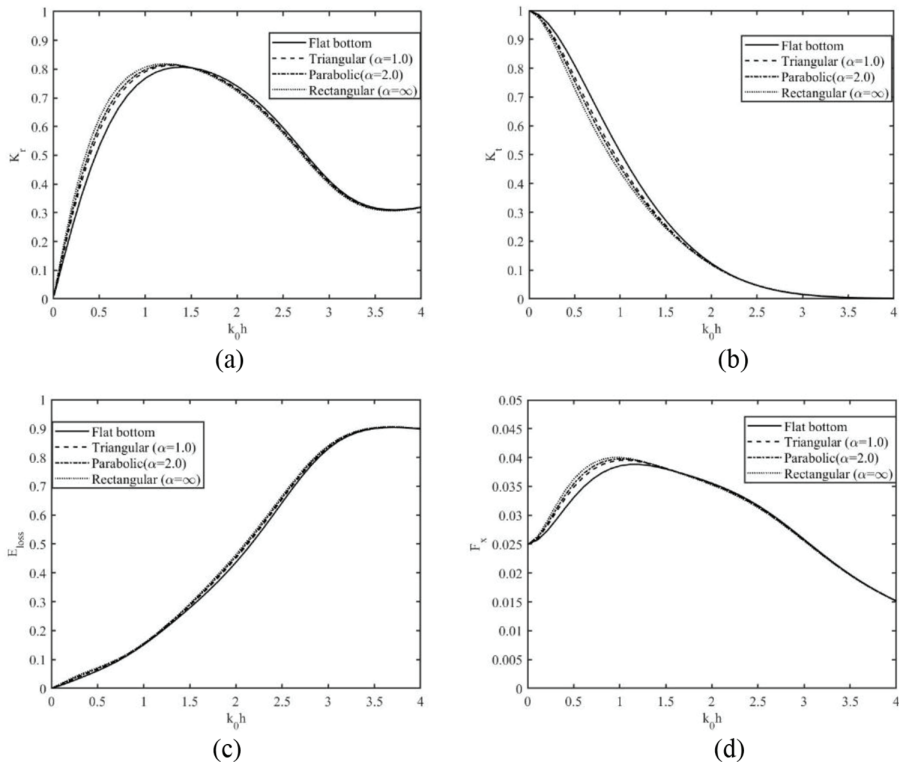
Figure 4: Variations of (a) K_r, (b) K_t, (c) E_{loss}, and (d) F_x versus $k_0 h$ for different types of bottom topography.

5.4 Effect of the submergence depth of the porous breakwater system

In Figs. 5(a)–(e), K_r, K_t, E_{loss}, F_z and F_x versus w_1/λ (λ is the wavelength corresponding to the incoming wave) are plotted for distinct submergence drafts of the breakwater system. It is observed that K_r, K_t, E_{loss}, F_x and F_z follow a periodic oscillatory trend as w_1/λ increases. This periodic nature is due to the formation of standing waves in the region between the slatted screens and the porous structure. Figure 5(a) shows that K_r reduces as the submergence depth of the breakwater system increases. This happens due to the fact that a major part of the incident wave energy is attenuated by the porous breakwater system, as seen in Fig. 5(c). Figure 5(b) depicts that K_t decreases significantly with an increase in the submergence draft of the porous breakwater system. It is seen that ≥ 98% of the incident wave energy is attenuated with 20% porosity of screens and having submergence draft $d = 0.65\ h$, and 15% porosity of the porous rectangular structure in the presence of parabolic sill. Further, Fig. 5(d) depicts that the dimensionless vertical force F_z reduces with an increase in the submergence depth of the breakwater system. However, contradictory behavior is observed in the case of the horizontal force F_x. This happens as the incident waves will hit over more areas of the slotted screens with an increase in the submergence depth. In both Figs. 5(d) and (e), the maximum wave forces are observed within the vicinity of $w_1/\lambda \approx n/2$, $n = 1,2,3, \ldots$ and the minimum wave forces acting on the porous rectangular structure are observed within the vicinity of $(n-1)/2 < w_1/\lambda < n/2$, $n = 1,2,3, \ldots$ for different submergence drafts of the breakwater system.
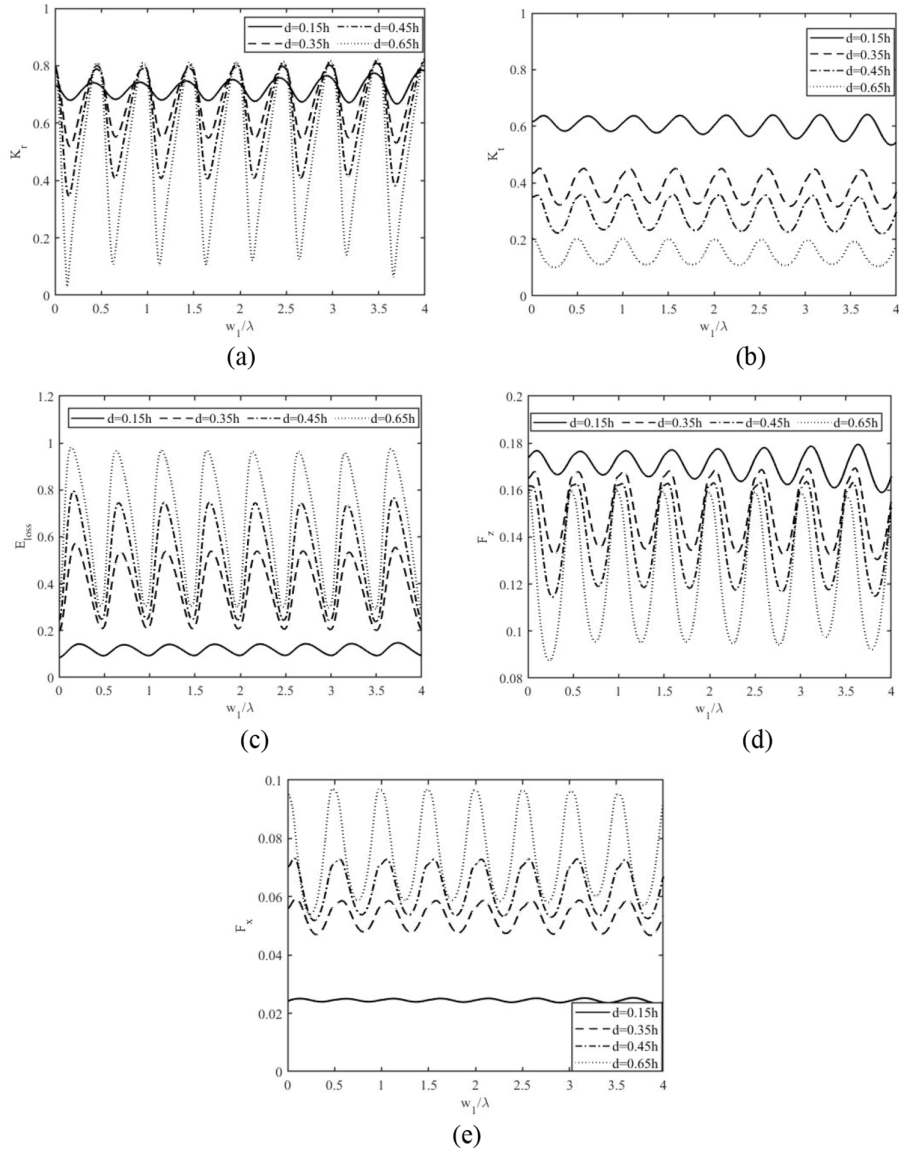
Figure 5: Variations of (a) K_r, (b) K_t, (c) E_{loss}, and (d) F_z, and (e) F_x versus w_1/λ for different submergence drafts of the breakwater system $\frac{d}{h}$ with $\epsilon_1 = \epsilon_2 = 0.2$, $\epsilon = 15\%$, $k_0 h = 1.0$, and $\theta = 0°$ over a parabolic sill.

5.5 Time-dependent free surface elevation

Using eqn (20), the time-dependent free surface elevation $\zeta(x, t)$ in regions 1, 2, 3, and 4 is obtained using the following Fourier integral:

$$\zeta(x,t) = Re\left\{\int_{-\infty}^{\infty} F(\sigma)\eta(x,\sigma)e^{-i\sigma t}\,d\sigma\right\}, \tag{21}$$

where

$$F(\sigma) = \sqrt{\frac{b}{\pi}} \exp\left(-b\left(\sigma - \sigma_0\right)\right)^2$$

is the FT (Fourier transform) of the incident pulse with b being the scale factor and σ_0 being the central frequency of the incident pulse. Further, $\eta(x, \sigma)$ is the frequency-dependent free surface elevation in regions 1, 2, 3, and 4. The time-dependent motion is shown in Figs. 6(a)–(g) for a different time. In all the figures, it is observed that a mixed interference contains the mix of both constructive and destructive interference due to the interaction of reflected waves by breakwater system and seabed undulation at various points. Since the interacting waves do not have the same wavelength, it is observed that occurrence of the constructive interference at some points and the occurrence of the destructive interference at some other points. The results show an irregular wave pattern in the seaside of the breakwater for waves with small and large wave periods. On the contrary, the resonance phenomena are observed due to the interaction between the incident and high-amplitude reflected waves by the breakwater system and seabed undulation.

6 CONCLUSIONS

An iterative BEM-based numerical solution approach has been introduced to analyze the effectiveness of porous floating breakwater with slotted screens over a sill-type bottom topography. The scattering coefficients such as the reflection and transmission coefficients, energy loss coefficient, and wave loads acting on the breakwater system are analyzed based on the linear wave–structure interaction theory. Moreover, the numerical results show a good agreement between the present results and the results of Abul-Azm and Gesraha [23] for the oblique wave scattering by a rigid rectangular floating breakwater over a horizontal seabed. The results depict that

- The scattering coefficients and wave forces on the floating porous breakwater system show a periodic oscillatory pattern as w_1/λ varies.
- The reflection coefficient increases with an increase in the angle of incidence in the long-wave regime. In case of normal incidence, ≥90% of the incident wave energy is attenuated with 20% porosities of the slotted screens and 15% porosity of the porous structure for a certain range of wave frequencies when the breakwater system is floating over a parabolic sill-type bottom, especially, for intermediate and shortwave regimes.
- Due to the presence of the slotted screens with moderate porosity, the wave load intensity on the rectangular porous structure reduces.
- The maximum wave forces are observed when $w_1/\lambda \approx n/2$, $n = 1,2,3, \ldots$, and the minimum wave forces acting on the porous rectangular structure are observed in the intermediate points $(n-1)/2 < w_1/\lambda < n/2$, $n = 1,2,3, \ldots,$ for different submergence drafts of the breakwater system when the breakwater system is floating over a parabolic sill.
- The maximum wave reflection and minimum wave transmission are noticed for porous breakwater systems with rectangular sill-type bottom profiles, in particular, for long waves.

Therefore, the proposed porous breakwater design helps to create the required tranquility zone in harbors by restricting the wave transmission and reducing the wave loads on the breakwater. Further, the present solution method can be extended to deal with various problems that arise in ocean and harbor engineering.
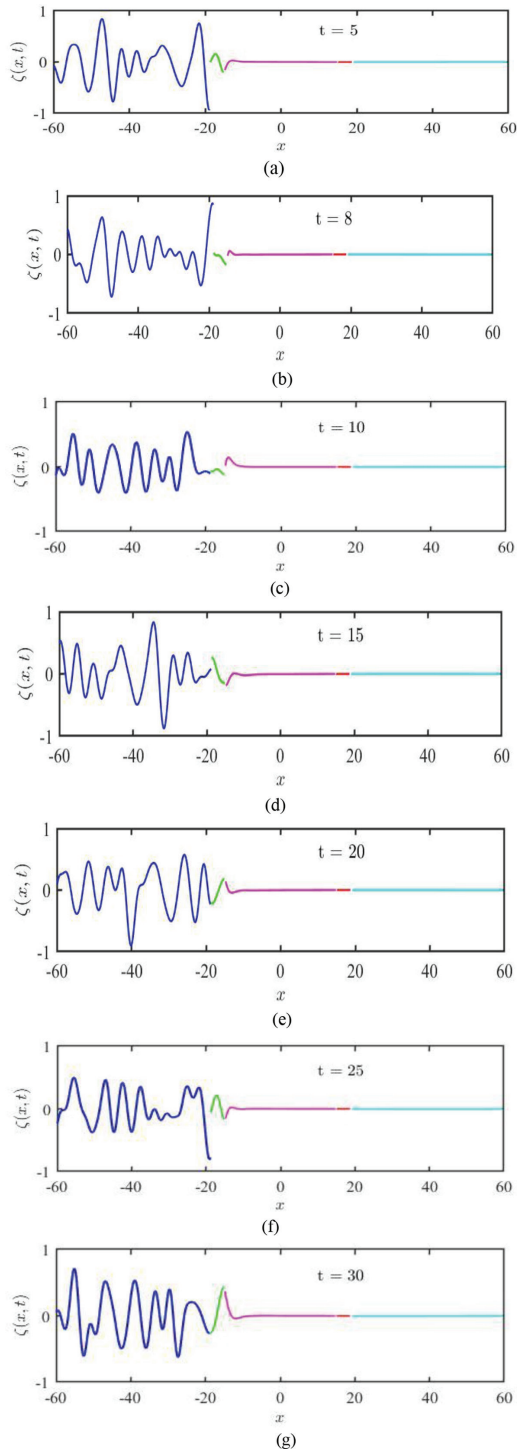
Figure 6: $\zeta(x, t)$ versus x for different time, (a) $t = 5$, (b) $t = 8$, (c) $t = 10$, (d) $t = 15$, (e) $t = 20$, (f) $t = 25.0$, and (g) $t = 30$ over a parabolic sill for $\theta = 0°$.

REFERENCES
[1] Yu, X., & Chwang, A.T. Wave motion through porous structures. *Journal of Engineering Mechanics*, **120(5)**, pp. 989–1008, 1994. https://doi.org/10.1061/(ASCE)0733-9399(1994)120:5(989)

[2] Koley, S., Panduranga, K., Almashan, N., Neelamani, S., & Al-Ragum, A., Numerical and experimental modeling of water wave interaction with rubble mound offshore porous breakwaters. *Ocean Engineering*, **218**, 108218. 2020. https://doi.org/10.1016/j.oceaneng.2020.108218

[3] Tabssum, S., Kaligatla, R.B., & Sahoo, T., Surface gravity wave interaction with a partial porous breakwater in the presence of bottom undulation. *Journal of Engineering Mechanics*, **146(9)**, 04020088, 2020. https://doi.org/10.1061/(ASCE)EM.1943-7889.0001818

[4] Hu, H., Wang, K.H., & Williams, A.N., Wave motion over a breakwater system of a horizontal plate and a vertical porous wall. *Ocean Engineering*, **29(4)**, pp. 373–386, 2002. https://doi.org/10.1016/S0029-8018(01)00029-4

[5] Deng, Z., Wang, L., Zhao, X., Huang, Z. Hydrodynamic performance of a T-shaped floating breakwater. *Applied Ocean Research*, **82**, pp. 325–336, 2019. https://doi.org/10.1155/2021/2944466

[6] Koley, S., Panduranga, K., Almashan, N., Neelamani, S., & Al-Ragum, A., Numerical and experimental modeling of water wave interaction with rubble mound offshore porous breakwaters. *Ocean Engineering*, **218**, 108218, 2020. https://doi.org/10.1016/j.oceaneng.2020.108218

[7] Koley, S., & Panduranga, K., Energy balance relations for flow through thick porous structures. *International Journal of Computational Methods and Experimental Measurements*, **9(1)**, pp. 28–37, 2021. https://doi.org/10.2495/CMEM-V9-N1-326-340

[8] Mei, C.C., & Jared, L.B., Scattering of surface waves by rectangular obstacles in waters of finite depth. *Journal of Fluid Mechanics*, **38(3)**, pp. 499–511, 1969. https://doi.org/10.1017/S0022112069000309

[9] Huang, L.H., & Chao, H.I., Reflection and transmission of water wave by porous breakwater. *Journal of Waterway, Port, Coastal, And Ocean Engineering*, **118(5)**, pp. 437–452, 1992. https://doi.org/10.1061/(ASCE)0733-950X(1992)118:5(437)

[10] Zhu, S, & Chwang, A.T., Analytical study of porous wave absorber. *Journal of Engineering Mechanics*, **127(4)**, pp. 326–332, 2001. https://doi.org/10.1061/(ASCE)0733-9399(2001)127:4(326)

[11] Li, Y., Liu, Y., & Bin, T., Porous effect parameter of thin permeable plates. *Coastal Engineering Journal*, **48(4)**, pp. 309–336, 2006. https://doi.org/10.1142/S0578563406001441

[12] Tsai, C.P., Chen, H.B., & Lee, F.C., Wave transformation over submerged permeable breakwater on porous bottom. *Ocean Engineering*, **33(11–12)**, pp. 1623–1643, 2006. https://doi.org/10.1016/j.oceaneng.2005.09.006

[13] Wiryanto, L.H., Wave propagation passing over a submerged porous breakwater. *Journal of Engineering Mathematics,* **70(1)**, pp. 129–136, 2011. https://doi.org/10.1007/s10665-010-9419-3

[14] Wang, H. Y., & Sun, Z. C., Experimental study of a porous floating breakwater. *Ocean Engineering*, **37(5–6)**, pp. 520–527, 2010. https://doi.org/10.1016/j.oceaneng.2009.12.005

[15] Liu, Y., & Li, H. J., Wave reflection and transmission by porous breakwaters: A new analytical solution. *Coastal engineering*, **78**, pp. 46–52, 2013. https://doi.org/10.1016/j.coastaleng.2013.04.003

[16] Koley, S., Behera, H., & Sahoo, T., Oblique wave trapping by porous structures near a wall. *Journal of Engineering Mechanics*, **141(3)**, 04014122, 2015. https://doi.org/10.1061/(ASCE)EM.1943-7889.0000843

[17] Shen, Y.M., Zheng, Y.H., & You, Y. G., On the radiation and diffraction of linear water waves by a rectangular structure over a sill. Part I. Infinite domain of finite water depth. *Ocean Engineering*, **32(8–9)**, pp. 1073–1097, 2005. https://doi.org/10.1016/j.oceaneng.2004.07.011

[18] Liu, X., Wang, X., Xu, S., & Ding, A., Influences of a varying sill at the seabed on two-dimensional radiation of linear water waves by a rectangular buoy. *Journal of Offshore Mechanics and Arctic Engineering*, **142(4)**, 2020. https://doi.org/10.1016/JOCEAN-ENG.2005.09.006

[19] Panduranga, K., Koley, S., & Sahoo, T., Surface gravity wave scattering by multiple slatted screens placed near a caisson porous breakwater in the presence of seabed undulations. *Applied Ocean Research*, **111**, 102675, 2021. https://doi.org/10.1016/j.apor.2021.102675

[20] Liu, Y., & Li, H.J., Iterative multi-domain BEM solution for water wave reflection by perforated caisson breakwaters. *Engineering Analysis with Boundary Elements*, **77**, pp. 70–80, 2017. https://doi.org/10.1016/j.enganabound.2016.12.011

[21] Sollitt, C.K., & Cross, R.H., Wave transmission through permeable breakwaters. In *Coastal Engineering*, **1972**. pp. 1827–1846, 1973. https://doi.org/10.9753/icce.v13.99

[22] Panduranga, K., & Koley, S. Mitigation of wave loads on the floating porous structure by slotted screens. *WIT Transactions on Engineering Sciences*, **131**, WIT Press, 2021, ISSN: 2046-0546. https://doi.org/10.2495/BE440091

[23] Abul-Azm, A.G., & Gesraha, M.R. Approximation to the hydrodynamics of floating pontoons under oblique waves. *Ocean Engineering*, **27(4)**, pp. 365–384, 2000. https://doi.org/10.1016/S0029-8018(98)00057-2

[24] Pozrikidis, C. A practical guide to boundary element methods with the software library BEMLIB. *CRC Press*, 2002.

[25] Chwang, A. T., & Chan, A. T., Interaction between porous media and wave motion. *Annual Review of Fluid Mechanics*, **30(1)**, pp. 53–84, 1998. https://doi.org/10.1146/annurev.fluid.30.1.53

[26] Panduranga, K., & Santanu, K., Water waves scattering by cylindrical dual porous floating breakwaters connected with a rectangular porous box and floating over an undulated seabed. *Meccanica*, **56(12)**, pp. 3001–3024, 2021.

[27] Wang, C.D., & Meylan, M.H. The linear wave response of a floating thin plate on water of variable depth. *Applied Ocean Research,* **24(3)**, pp.163–174, 2002. https://doi.org/10.1016/S0141-1187(02)00025-1